PASJ: Publ. Astron. Soc. Japan , 1–??,

Planetary Companions to Three Evolved Intermediate-Mass Stars: HD 2952, HD 120084, and ω Serpentis

Bun'ei Sato,[1] Masashi Omiya,[1] Hiroki Harakawa,[1] Yu-Juan Liu, [2] Hideyuki Izumiura,[3,4] Eiji Kambe,[3] Yoichi Takeda,[4,5] Michitoshi Yoshida,[6] Yoichi Itoh,[7] Hiroyasu Ando,[4,5] Eiichiro Kokubo[4,5] and Shigeru Ida[1]

[1] *Department of Earth and Planetary Sciences, Tokyo Institute of Technology, 2-12-1 Ookayama, Meguro-ku, Tokyo 152-8551, Japan*

satobn@geo.titech.ac.jp

[2] *Key Laboratory of Optical Astronomy, National Astronomical Observatories, Chinese Academy of Sciences, Beijing 100012, China*

[3] *Okayama Astrophysical Observatory, National Astronomical Observatory of Japan, Kamogata, Okayama 719-0232, Japan*

[4] *The Graduate University for Advanced Studies, Shonan Village, Hayama, Kanagawa 240-0193, Japan*

[5] *National Astronomical Observatory of Japan, 2-21-1 Osawa, Mitaka, Tokyo 181-8588, Japan*

[6] *Hiroshima Astrophysical Science Center, Hiroshima University, Higashi-Hiroshima, Hiroshima 739-8526, Japan*

[7] *Nishi-Harima Astronomical Observatory, Center for Astronomy, University of Hyogo, 407-2, Nishigaichi, Sayo, Hyogo 679-5313, Japan*

(Received ; accepted)

Abstract

We report the detections of planetary companions orbiting around three evolved intermediate-mass stars from precise radial velocity measurements at Okayama Astrophysical Observatory. HD 2952 (K0III, $2.5M_\odot$) and ω Ser (G8III, $2.2M_\odot$) host a relatively low mass planet with minimum mass of $m_2 \sin i = 1.6$ $M_{\rm J}$ and 1.7 $M_{\rm J}$ in nearly circular orbits with period of $P = 312$ and 277 d, respectively. HD 120084 (G7 III, $2.4M_\odot$) hosts an eccentric planet with $m_2 \sin i = 4.5$ $M_{\rm J}$ in an orbit with $P = 2082$ d and eccentricity of $e = 0.66$. The planet has one of the largest eccentricities among those ever discovered around evolved intermediate-mass stars, almost all of which have eccentricity smaller than 0.4. We also show that radial velocity variations of stellar oscillations for G giants can be averaged out below a level of a few m s^{-1} at least in timescale of a week by high cadence observations, which enables us to detect a super-Earth and a Neptune-mass planet in short-period orbits even around such giant stars.

Key words: stars: individual: HD 2952 — stars: individual: HD 120084 — stars: individual: ω Ser — planetary systems — techniques: radial velocities

1. Introduction

Planets and brown dwarfs discovered around intermediate-mass stars (1.5–5$M_\odot$) have been growing in number for the last decade. Hundreds of GK giants and subgiants, which are evolved counterparts of intermediate-mass BA dwarfs, have been intensively surveyed in radial velocity by utilizing their spectral features appropriate to precise radial velocity measurements (e.g., Frink et al. 2002; Setiawan et al. 2005; Hatzes et al. 2005; Hatzes et al. 2006; Lovis & Mayor 2007; Niedzielski et al. 2009b; Döllinger et al. 2009; de Medeiros et al. 2009; Sato et al. 2010; Johnson et al. 2011a; Wang et al. 2012; Wittenmyer et al. 2011; Omiya et al. 2012; Lee et al. 2012; Sato et al. 2013). More than 50 substellar companions have been discovered around such evolved intermediate-mass stars, which are ranging from 0.6 to 40 $M_{\rm J}$ in minimum mass, from 0.08 to 6 AU in semimajor axis, and from 0 to 0.68 in eccentricity. Planets less massive than $2M_{\rm J}$ were mostly found around subgiants because giants normally show larger stellar jitter of 10–20 m s^{-1} making detection of low mass planets more difficult (e.g., Sato et al. 2005), and all of the companions except for only one hot-Jupiter around a subgiant (Johnson et al. 2010) were found in orbits beyond 0.6 AU. Not only single planets but also multiple-planet systems have been found, some of which are in mean-motion resonance (Johnson et al. 2011b; Niedzielski et al. 2009a; Niedzielski et al. 2009b; Sato et al. 2012; Sato et al. 2013). Recently direct imaging succeeded in detecting substellar companions in wide orbits around BA dwarfs, which are complementary to radial velocity observations (e.g., Marois et al. 2008; Carson et al. 2013). The orbital properties of these companions now serve as test cases for general understanding of formation and evolution of substellar companions around intermediate-mass stars (e.g., Currie 2009).

The Okayama Planet Search Program is one of the long-continued planet search programs and has been regularly monitoring radial velocities of about 300 intermediate-mass GK giants since 2001 at Okayama Astrophysical Observatory (OAO) in Japan (Sato et al. 2005). A total of 20 planets and 6 brown dwarfs have been discovered so far at OAO including those found in collaboration with Xinglong observatory in China, Bohyunsan Optical Astronomy Observatory in Korea, Subaru 8.2m telescope

in Hawaii, and Australian Astronomical Observatory. (e.g., Sato et al. 2012; Omiya et al. 2012; Wang et al. 2012; Sato et al. 2010; Sato et al. 2013).

From the planet search program, here we report the discovery of three new planetary companions around GK giants. Rest of the paper is organized as follows. We describe the observations in section 2 and the stellar properties are presented in section 3. Analyses of radial velocity, period search, orbital solution, stellar activity, and line shape variation are described in section 4 and the results are presented in section 5. Section 6 and 7 are devoted to discussion and summary, respectively.

2. Observation

All of the observations were made with the 1.88 m reflector and the HIgh Dispersion Echelle Spectrograph (HIDES; Izumiura 1999) at OAO. In 2007 December, HIDES was upgraded from single CCD (2K×4K) to a mosaic of three CCDs, which enables us to simultaneously obtain spectra with a wavelength range of 3750–7500Å using a red cross-disperser. Furthermore, the high-efficiency fiber-link system with an image slicer has been available for HIDES since 2010, which makes overall throughput more than twice than that with the conventional slit observations (Kambe et al. 2013). We basically obtained the data presented in this paper using the slit (hereafter HIDES-Slit) mode, but we also used the fiber-link (hereafter HIDES-Fiber) mode for two of the three stars.

In the HIDES-Slit mode, the slit width was set to 200 μm ($0.76''$) giving a spectral resolution ($R = \lambda/\Delta\lambda$) of 67000 by about 3.3 pixels sampling. In the HIDES-Fiber mode, the width of the sliced image is $1.05''$ corresponding to a spectral resolution of R =55000 by about 3.8 pixels sampling. Each observing mode uses its own iodine absorption cell (I_2 cell; Kambe et al. 2002; Kambe et al. 2013) for precise radial velocity measurements, which provides a fiducial wavelength reference in a wavelength range of 5000–5800Å. Possible offset in radial velocities between the two modes caused by using the different I_2 cells is treated as a free parameter in orbital fitting (see section 4.3).

The reduction of echelle data (i.e. bias subtraction, flat-fielding, scattered-light subtraction, and spectrum extraction) is performed using the IRAF[1] software package in the standard way.

3. Stellar Properties

Atmospheric parameters (effective temperature $T_{\rm eff}$, surface gravity $\log g$, micro-turbulent velocity v_t, Fe abundance [Fe/H], and projected rotational velocity $v \sin i$) of all the targets for Okayama Planet Search Program were derived by Takeda et al. (2008), based on the measured equivalent widths of well-behaved Fe I and Fe II lines of iodine-free stellar spectra. Details of the procedure and resultant parameters are presented in Takeda et al. (2002) and Takeda et al. (2008).

They also obtained the absolute magnitude M_V of each star from the apparent V-band magnitude and Hipparcos parallax π (ESA 1997) correcting interstellar extinction A_V from Arenou et al. (1992)'s table, and obtained the bolometric correction $B.C.$ based on the Kurucz (1993)'s theoretical calculation. The luminosity L and mass M of each star were derived using these parameters and theoretical evolutionary tracks of Lejeune & Schaerer (2001), and the stellar radius R was derived by the Stefan-Boltzmann relationship and the measured L and $T_{\rm eff}$. The properties of the three stars presented in this paper (HD 2952, HD 120084, ω Ser) are summarized in table 1, and the stars are plotted on the HR diagram in figure 1.

The three stars are known to be stable in photometry to a level of $\sigma_{\rm HIP} = 0.005 - 0.007$ mag (ESA 1997), and they are chromospherically inactive with no significant emission in the core of Ca II HK lines as shown in figure 2. Since we can obtain spectra covering Ca II HK lines together with radial velocity data after installing 3 CCDs in 2007, we use the lines to check stellar chromospheric activity correlated with radial velocity variations (see section 4.4).

4. Analysis

4.1. Radial Velocity

Radial velocity analysis was carried out using the modeling technique of an I_2-superposed stellar spectrum detailed in Sato et al. (2002) and Sato et al. (2012), which is based on the method by Butler et al. (1996). In the technique, an I_2-superposed stellar spectrum is modeled as a product of a high resolution I_2 and a stellar template spectrum convolved with a modeled instrumental profile (IP) of the spectrograph. We here used a stellar template that was obtained by deconvolving a pure stellar spectrum with the spectrograph IP estimated from an I_2-superposed B-star or Flat spectrum. We applied the stellar template thus obtained with HIDES-Slit mode observations to radial velocity analysis for the data taken with HIDES-Fiber mode as well as HIDES-Slit mode. We took account of a velocity offset, $\Delta{\rm RV}_{\rm f-s}$, between the two observing modes as a free parameter when we determine orbital parameters (see section 4.3). Measurement error in radial velocity was estimated from an ensemble of velocities from each of ∼300 spectral regions (each ∼3Å long) in every exposure.

4.2. Period Search

A Lomb-Scargle periodogram analysis (Scargle 1982) was performed to search for periodicity in radial velocity data, and False Alarm Probability (FAP) was estimated to assess the significance of the periodicity. To estimate the FAP, we created 10^5 fake datasets, in which the observed radial velocities were randomly redistributed, keeping fixed the observation time, and applied the same periodogram analysis to them. The fraction of fake datasets

[1] IRAF is distributed by the National Optical Astronomy Observatories, which is operated by the Association of Universities for Research in Astronomy, Inc. under cooperative agreement with the National Science Foundation, USA.

exhibiting a periodogram power higher than the observed one was adopted as a FAP for the signal.

4.3. Keplerian Orbital Solution by MCMC Method

Keplerian orbital model for the radial velocity data and uncertainties for the parameters were derived using the Bayesian Markov chain Monte Carlo (MCMC) method (e.g., Ford 2005; Gregory 2005; Ford & Gregory 2007). Since the details of the method are presented in the literatures, we here briefly describe the procedure and parameters for the model adopted in this paper.

In Bayes' theorem, the target joint probability distribution, the posterior probability distribution, for parameters $\boldsymbol{\theta}$ of a certain model M based on observational data $\boldsymbol{d}$ and prior background information I is given by

$$p(\boldsymbol{\theta}|\boldsymbol{d},I,M) = Cp(\boldsymbol{\theta}|I,M) \times p(\boldsymbol{d}|\boldsymbol{\theta},I,M) \quad (1)$$

where C is the normalization constant, $p(\boldsymbol{\theta}|I,M)$ is the prior probability distribution of $\boldsymbol{\theta}$, and $p(\boldsymbol{d}|\boldsymbol{\theta},I,M)$ is the likelihood, which is the probability that we would have obtained the data $\boldsymbol{d}$ given the parameters $\boldsymbol{\theta}$, model M, and priors I.

The likelihood function is given by

$$p(\boldsymbol{d}|\boldsymbol{\theta},I,M) = A\exp\left[\sum_j \sum_{i=1}^{N_j} \frac{(v_{i,j}-y_{i,j})^2}{2\left(\sigma_{i,j}^2+s_j^2\right)}\right] \quad (2)$$

$$A = \prod_j (2\pi)^{-N_j/2} \prod_{i=1}^{N_j} \left(\sigma_{i,j}^2+s_j^2\right)^{-1/2} \quad (3)$$

where N_j is the number of data points for the jth instrument, $\sigma_{i,j}$ is the measurement uncertainties for each point, $v_{i,j}$ and $y_{i,j}$ are observed and modeled radial velocities, respectively. Extra Gaussian noise s_j is incorporated for observations with jth instrument, including intrinsic stellar jitter such as stellar oscillation and unknown noise source, in addition to the measurement uncertainties.

For a single planet, reflex motion in stellar radial velocity at time t_i observed with jth instrument can be expressed as

$$y_{i,j}(t_i) = V_j + K_1[\sin(f_i+\omega) + e\sin\omega] \quad (4)$$

where V_j is systematic velocity with reference to jth instrument, K_1, ω, e, and P is velocity semiamplitude, argument of periastron, eccentricity, and orbital period, respectively. f_i is true anomaly of the planet at t_i, which is a function of e, P, and time of periastron passage T_p. Instead of T_p, we here adopted χ, fraction of an orbit of the planet prior to the start of data taking, at which periastron occurred.

For the prior probability distribution, we follwed Ford & Gregory (2007) adopting Jeffrey's prior for P, modified Jeffrey's prior for K_1 and s_j, and uniform one for other parameters. Then, joint prior for the model parameters, assuming independence, is given by

$$\begin{aligned} p(\boldsymbol{\theta}|I,M) &= p(P|I,M)p(K_1|I,M)p(e|I,M)p(\omega|I,M) \\ &\times p(\chi|I,M)\prod_j p(V_j|I,M)p(s_j|I,M) \\ &= \frac{1}{P\ln(P_{max}/P_{min})}\frac{1}{(K_1+K_a)\ln[(K_a+K_{max})/K_a]} \\ &\times \frac{1}{2\pi}\prod_j \frac{1}{V_{j,max}-V_{j,min}}\frac{1}{(s_j+s_a)\ln[(s_a+s_{max})/s_a]} \end{aligned} \quad (5)$$

The parameter priors we adopted are summarized in table 2.

The posterior probability distribution was obtained with the MCMC method, which uses a stochastic process to generate a "chain" of points in parameter space that approximates the desired probability distribution. The chain is derived from an initial point by iterating a "jump function", which was the addition of a Gaussian random number to each parameter value in our case. If the new set of parameters $\boldsymbol{\theta'}$ has a larger posterior probability $p(\boldsymbol{\theta'}|\boldsymbol{d},I,M)$ than that for the previous set of parameters $p(\boldsymbol{\theta}|\boldsymbol{d},I,M)$, the jump is executed and the new parameters are accepted; if not, the jump is only executed with probability $p(\boldsymbol{\theta'}|\boldsymbol{d},I,M)/p(\boldsymbol{\theta}|\boldsymbol{d},I,M)$; otherwise, the previous parameters are recorded. We set the relative sizes of the Gaussian perturbations based on the 1σ uncertainties estimated on ahead with the bootstrap method, and required the overall acceptance rate of $\sim$25%, which is the total fraction of jumps executed, as recommended by Roberts et al. (1997). We generated 5 independent chains, each of which started from random initial values 5σ away from the best-fit ones. Each chain had 10^6–10^7 points, the first 10% or 500,000 of which were discarded to minimize the effect of the initial condition. To check the convergence and the consistency between the chains, we computed Gelman-Rubbin statistic (Gelman & Rubbin 1992) for each parameter, which is a comparison between the interchain variance and the intrachain variance, and confirmed that the results were within a few percent of unity, a sign of good mixing and convergence. We also calculated an estimate of the effective number of independent draws following Gelman et al. (2003) and confirmed that the value was larger than 1000. The resultant chains were merged to derive the final joint posterior probability distribution function (PDF). We derived the median value of the PDF for each parameter and set the 1σ uncertainty as the range between 15.87% and 84.13% of the PDF.

4.4. Stellar Activity

Rotational modulation of spots or activity cycle of stars cause apparent variations in stellar radial velocities, which can masquerade as a planetary signal (e.g., Queloz et al. 2001). Thus it is important to check the activity level of stars together with radial velocity variations. For this purpose, Ca II HK lines are widely used as activity indicators since the flux of the line cores is a good tracer of chromospheric activity (e.g., Duncan et al. 1991; Noyes et al. 1984). We here define Ca II H index S_H as

$$S_H = \frac{F_H}{F_B+F_R} \quad (6)$$

where F_H is a total flux in a wavelength bin 0.66Å wide centered on the H line, F_B and F_R are those in bins 1.1 Å wide centered on minus and plus 1.2 Å from the center

of the H line, respectively. By setting the reference wavelength bands, B and R, close to the base of the CaII H line core in this way, we tried to minimize the error in S_H caused by imperfect normalization of the continuum level. We obtained the S_H values only for spectra with S/N of F_H over ∼40 among those taken after 2007.

4.5. Line Shape Variation

To investigate other possible causes of apparent radial velocity variations rather than orbital motion, spectral line shape analysis was performed using IP-deconvolved stellar templates. Details of the analysis are described in Sato et al. (2007) and Sato et al. (2002), and here we briefly summarize the procedure.

At first, two IP-deconvolved templates were extracted from five I_2-superposed stellar spectra at nearly the phases of maximum and minimum in observed radial velocities using the technique by Sato et al. (2002). Cross correlation profiles of the two templates were then derived for about 100 spectral segments (4–5Å width each) that have no severely blended or broad lines in them. Three bisector quantities were calculated for the cross correlation profile for each segment: the velocity span (BVS), the velocity difference between two flux levels of the bisector; the velocity curvature (BVC), the difference of the velocity span of the upper and lower half of the bisector; and the velocity displacement (BVD), the average of the bisector at three different flux levels. Flux levels of 25%, 50%, and 75% of the cross correlation profile were used to calculate the above three quantities. Both the BVS and the BVC being identical to zero and the average BVD agreeing with the velocity difference between the two templates ($\simeq 2K_1$) suggest that the cross correlation profiles can be considered to be symmetric. Thus the observed radial velocity variations are considered to be caused by parallel shifts of the spectral lines rather than deformation of them, which favors the orbital motion hypothesis.

5. Results

5.1. HD 2952 (HR 135, HIP 2611)

We collected a total of 63 radial velocity data of HD 2952 between 2004 January and 2012 December using both of HIDES-Slit and HIDES-Fiber mode. We obtained a signal-to-noise ratio S/N=100–260 pix^{-1} at 5500Å with an exposure time 780–1800 sec using HIDES-Slit mode and S/N=200–320 pix^{-1} at 5500Å with an exposure time 450–900 sec using HIDES-Fiber mode.

The observed radial velocities are shown in figure 3 and are listed in table 3 together with their estimated uncertainties. Lomb-Scargle periodogram of the data exhibits a dominant single peak at a period of 313 days with $FAP = 1 \times 10^{-5}$.

The orbital parameters for single Keplerian model derived by MCMC method are $P = 311.6^{+1.7}_{-1.9}$ days, $K_1 = 26.3^{+3.8}_{-3.4}$ m s^{-1}, and $e = 0.129^{+0.099}_{-0.085}$, which are median and 68.3% credible regions for PDF. The resulting Keplerian model is shown in figure 3 overplotted on the velocities, whose error bars include the median value of the derived stellar jitter of $s_{\rm slit} = 13.3$ m s^{-1} and $s_{\rm fiber} = 6.5$ m s^{-1} for HIDES-Slit and HIDES-Fiber mode, respectively. The rms scatter of the residuals to the Keplerian fit was 12.4 m s^{-1} and we found no significant periodicity in the residuals at this stage, although some possible long-term trend is apparently seen. Adopting a stellar mass of 2.54 $M_\odot$, we obtain a minimum mass $m_2 \sin i = 1.6$ $M_{\rm J}$ and a semimajor axis $a = 1.2$ AU for the orbiting planet.

We did not find any significant variations in Ca II H index (figure 4) and spectral line profiles correlated with the orbital period (table 7).

5.2. HD 120084 (HR 5184, HIP 66903)

We obtained a total of 33 radial velocity data of HD 120084 between 2003 March and 2012 December using HIDES-Slit mode with S/N=75–230 pix^{-1} at 5500Å by an exposure time 900–1800 sec.

The observed radial velocities are shown in figure 5 and are listed in table 4 together with their estimated uncertainties. Lomb-Scargle periodogram of the data exhibits a peak at around a period of 1840 days. The FAP of peak is 0.06, which is not significant because of the long period, limited phase coverage, and deviation from sinusoidal curve for the radial velocity variations.

The single Keplerian model for the data and uncertainties for each orbital parameter were derived by MCMC method. The median values and the 68.3% credible regions for orbital parameters are $P = 2082^{+24}_{-35}$ d, $K_1 = 53^{+33}_{-11}$ m s^{-1}, and $e = 0.66^{+0.14}_{-0.10}$. The resulting model is shown in figure 5 overplotted on the velocities, whose error bars include stellar jitter of 5.0 m s^{-1}. The rms scatter of the residuals to the Keplerian fit was 5.8 m s^{-1} and we found no significant periodicity in the residuals. Adopting a stellar mass of 2.39 $M_\odot$, we obtain $m_2 \sin i = 4.5$ $M_{\rm J}$ and $a = 4.3$ AU for the companion. Figure 6 shows 2-dimensional PDF between K_1 and e. As seen in the figure, the parameters are not well constrained yet because the phase of velocity minimum was not covered by our observations. However, the companion minimum-mass is below 13 $M_{\rm J}$ with 99% confidence, then the companion still falls into the planetary regime.

We did not analyze Ca II H variations for the star because of the low S/N ratio for the core of the observed spectra. We did not find any significant variations in spectral line profiles correlated with the orbital period (table 7).

5.3. ω Serpentis (HR 5888, HD 141680, HIP 77578)

Probable periodic radial velocity variations of ω Ser were first reported in Sato et al. (2005) at an early time of the Okayama Planet Search Program. A total of 123 radial velocity data of ω Ser were collected between 2001 February and 2013 January with HIDES-Slit and HIDES-Fiber mode. We obtained S/N=80–340 pix^{-1} at 5500Å with an exposure time 480–1800 sec using HIDES-Slit mode and S/N=150–390 pix^{-1} at 5500Å with an exposure time 300–900 sec using HIDES-Fiber mode.

The observed radial velocities are shown in figure 7 and are listed in table 5 together with their estimated

uncertainties. Lomb-Scargle periodogram of the data exhibits a dominant peak at a period of 276 days with a $FAP < 1 \times 10^{-5}$.

The MCMC analysis for a single Keplerian model yielded the orbital parameters of $P = 277.02^{+0.52}_{-0.51}$ d, $K_1 = 31.8^{+2.3}_{-2.3}$ m s^{-1}, and $e = 0.106^{+0.079}_{-0.069}$, which are median and 68.3% credible regions for PDF. The resulting Keplerian model is shown in figure 7 overplotted on the velocities with error bars including the median value of the derived stellar jitter of $s_{\rm slit} = 18.7$ m s^{-1} and $s_{\rm fiber} = 10.4$ m s^{-1} for HIDES-Slit and HIDES-Fiber mode, respectively. The rms scatter of the residuals to the Keplerian fit was 17.0 m s^{-1} and we found no significant periodicity in the residuals at this stage. Adopting a stellar mass of 2.17 $M_\odot$, we obtain $m_2 \sin i = 1.7$ $M_{\rm J}$ and $a = 1.1$ AU for the orbiting planet.

We did not find any significant variations in Ca II H index (figure 8) and spectral line profiles correlated with the orbital period (table 7).

6. Discussion

6.1. Stellar Activity

We found no variations in S_H values correlated with radial velocity variations for HD 2952, HD 120084, and ω Ser suggesting that the observed radial velocity variations of these stars are not caused by stellar activity. In comparison, we also examined the variations of S_H values for a chromospherically active G-type giant HD 120048, which shows significant core reversal in the Ca II HK lines (see figure 2). Figure 9 shows the variations in S_H values for the star against radial velocity variations. It clearly shows that the radial velocity variations are correlated with activity level, indicating that the index can be used to investigate a cause of radial velocity variations.

We also performed spectral line shape analysis for HD 120048 in the same manner as those for other three stars. As presented in table 7, no significant variations are detected for the star along with the other three stars. It suggests that spectral line shape variations caused by rotational modulation are too small to be detected by the current method or the observed radial velocity variations in HD 120048 originate from atmospheric motion (expansion or contraction) that are not necessarily accompanied by significant line profile variations. The results demonstrate the importance of monitoring not only line profile variability but also chromospheric activity in order to investigate causes of radial velocity variations of GK giants. Further detailed study on the variability of HD 120048 is beyond the scope of this paper, which will be done in a forthcoming paper.

6.2. Detectability of Less Massive Planets around GK Giants

HD 2952 b ($m_2 \sin i = 1.6$ $M_{\rm J}$, $a = 1.2$ AU) and ω Ser b ($m_2 \sin i = 1.7$ $M_{\rm J}$, $a = 1.1$ AU) are the least massive planets ever discovered around intermediate-mass (1.5–5$M_\odot$) giants together with HD 100655 b ($m_2 \sin i = 1.7$ $M_{\rm J}$; Omiya et al. 2012) and o CrB b ($m_2 \sin i = 1.5$ $M_{\rm J}$; Sato et al. 2012). Less massive planets are also found around low-mass (<1.5$M_\odot$) K giants such as BD+48 738 b ($m_2 \sin i = 0.91$ $M_{\rm J}$, $a = 1.0$ AU; Gettel et al. 2012). It is normally more difficult to detect planets with $\lesssim 2 M_{\rm J}$ around such giants because of the relatively larger stellar jitter. However, these discoveries demonstrate that it is still possible to detect such less massive planets even around GK giants by high cadence observations.

How low mass planets are detectable around GK giants? Ando et al. (2010) conducted asteroseismic observations for some of the G giants in our sample and detected solar-like oscillations in them. The results show that the stellar jitter of the giants are primarily dominated by solar-like oscillations with periods of 3–10 hours and integrated velocity amplitudes of 10–20 m s^{-1}, which are consistent with jitters in longer timescale (e.g., Sato et al. 2005). In the case of solar-type dwarfs, the p-mode oscillations have much shorter periods ($\sim$ 10 minutes) and smaller velocity amplitudes (~ 1 m s^{-1}), which can be canceled out down to $\sim$20 cm s^{-1} by integration for ~ 15 minutes (e.g., Mayor & Udry 2008). Figure 10 demonstrates the benefit by applying the similar strategy to the radial velocity data presented in Ando et al. (2010). As seen in the figure, the scatters are reduced by a factor of 2–4 by binning the data over one night ($\sim$ 10 hr), which makes the detection limit of planets down to below 1 $M_{\rm J}$ at 1 AU and even super-Earth class planets in short period orbits around stars like η Her (G8III-IV). Although it takes time to apply this strategy to all of our targets and the jitters may have various time scales in variations, the results show that we can potentially reduce the detection limit of planets around giants if we mitigate the effect of stellar jitters by proper observational strategy.

6.3. An Eccentric Planet: HD 120084 b

HD 120084 b ($m_2 \sin i = 4.5$ $M_{\rm J}$, $a = 4.3$ AU) is a long-period eccentric planet. The eccentricity exceeds 0.4 with the 99% confidence, while almost all the planets discovered around evolved intermediate-mass stars have eccentricity below 0.4 (figure 11). Several scenarios have been proposed for the origin of eccentric planets including planet-planet scattering (e.g., Marzari & Weidenschilling 2002; Jurić & Tremaine 2008; Ford & Rasio 2008) and secular perturbations by an outer body (e.g., Holman et al. 1997; Mazeh et al. 1997; Takeda & Rasio 2005), in both of which we can expect to find a distant companion. In order to explore such a possible distant companion around HD 120084, we performed MCMC analysis for a single Keplerian model with a linear velocity trend $\dot{\gamma}$. As a result, we constrained the velocity trend to be $|\dot{\gamma}| < 2$ m s^{-1} yr^{-1} with 99% confidence, giving an order-of-magnitude relation (e.g., Winn et al. 2009)

$$\frac{m_{\rm c} \sin i_{\rm c}}{a_{\rm c}^2} \sim \frac{\dot{\gamma}}{G} < 0.01 \ M_{\rm J} \ {\rm AU}^{-2} \qquad (7)$$

where m_c is the companion mass, i_c is the orbital inclination, and a_c is the orbital radius. The result could exclude existence of a brown-dwarf companion (≥ 13 $M_{\rm J}$) within $\sim$36 AU and a stellar one (≥ 80 $M_{\rm J}$) within $\sim$90 AU.

It may also be possible to assume that (unobserved) another body was scattered into inner orbit and then engulfed by the central star. Recently Adamow et al. (2012) reported a possible example for this case; BD+48 740, a lithium rich giant with a possible planetary companion in an eccentric and long-period orbit. It has been proposed for years that the planet engulfment scenario is an origin of existence of lithium overabundant giants (e.g., Siess & Livio 1999), and Adamow et al. suggested that BD+48 740 might be the case. We determined lithium abundance $A(\mathrm{Li})$[2] for HD 120084 using the spectral synthesis method with the IDL/Fortran SIU software package developed by Reetz (1993, private communication). The synthetic spectrum is presented by a single Gaussian profile, convolved with the broadening function of stellar rotation, macroturbulence and instrumental profile. The lithium abundance is obtained by fitting the synthetic spectrum for ^{7}Li 6708Å to the observed one with the contribution of the line of FeI 6707.467Å taken into account. We then obtained $A(\mathrm{Li}) \leq 0.37$ for HD 120084, which does not exhibit overabundance of lithium compared with other giants in our sample. Details of the procedure as well as lithium abundances for other targets of our planet-search survey can be found in Liu et al. (in preparation).

7. Summary

Here we reported three new planetary systems around evolved intermediate-mass stars from precise radial velocity measurements at OAO. These add to the diversity of planets around evolved intermediate-mass stars in terms of less massive planets than 2 M_{J} (HD 2952 b, ω Ser b) and a highly eccentric planet with $e = 0.66$ (HD 120084 b).

The Okayama Planet Search Program has been continuously monitoring radial velocity of about 300 GK giants for 12 years, which corresponds to orbital semimajor axis of 6.5 AU around $2M_{\odot}$ stars. Furthermore, since 2010, the high-efficiency fiber-link system for HIDES has been available. The improvement in efficiency allows us to observe each star more frequently, which helps to push down the detection limit of planets. The continuous observations combined with the frequent sampling will further uncover both long-period and less-massive planets around evolved intermediate-mass stars.

This research is based on data collected at Okayama Astrophysical Observatory (OAO), which is operated by National Astronomical Observatory of Japan (NAOJ). We are grateful to all the staff members of OAO for their support during the observations. We thank students of Tokyo Institute of Technology and Kobe University for their kind help for the observations. BS was partly supported by MEXT's program "Promotion of Environmental Improvement for Independence of Young Researchers" under the Special Coordination Funds for Promoting Science and Technology and by Grant-in-Aid for Young Scientists (B) 20740101 from the Japan Society for the Promotion of Science (JSPS). BS is supported by Grant-In-Aid for Scientific Research (C) 23540263 from JSPS and HI is supported by Grant-In-Aid for Scientific Research (A) 23244038 from JSPS. YJL is supported by the National Natural Science Foundation of China under grants 11173031. This research has made use of the SIMBAD database, operated at CDS, Strasbourg, France.

[2] $A(\mathrm{Li}) = \log n_{\mathrm{Li}}/n_{\mathrm{H}} + 12$

References

Adamow, M., Niedzielski, A., Villaver, E., Nowak, G., & Wolszczan, A. 2012, ApJ, 754, 15
Ando, H., Tsuboi, Y., Kambe, E., & Sato, B. 2010, PASJ, 62, 1117
Arenou, F., Grenon, M., & Gomez, A. 1992, A&A, 258, 104
Bowler, B.P., et al., ApJ, 710, 1365
Butler, R. P., Marcy, G. W., Williams, E., McCarthy, C., Dosanjh, P., & Vogt, S. S. 1996, PASP, 108, 500
Carson, J. et al., ApJ, 763, 32
Currie, T. 2009, ApJ, 694, 171
de Medeiros, J.R., et al., A&A, 504, 617
Duncan, D.K. et al. 1991, ApJS, 76, 383
Döllinger, M.P., Hatzes, A.P., Pasquini, L., Guenther, E.W., & Hartmann, M. 2009, A&A, 505, 1311
ESA. 1997, The *Hipparcos* and Tycho Catalogues (ESA SP-1200; Noordwijk: ESA)
Ford, E.B. 2005, AJ, 129, 1706
Ford E. B., Gregory P. C., 2007, in Babu G. J., Feigelson E. D., eds, ASP Conf. Ser. Vol. 371, Statistical Challenges in Modern Astronomy IV. Astron. Soc. Pac., San Francisco, p. 189
Ford, E.B. & Rasio, F.A. 2008, ApJ, 686, 621
Frink, S., Mitchell, D.S., Quirrenbach, A., Fischer, D., Marcy, G.W., & Butler, R.P. 2002, ApJ, 576, 478
Gelman, A., Carlin, J.B., Stern, H.S. & Rubin, D.B. 2003, Bayesian Data Analysis (2nd ed.; Boca Raton: Chapman & Hall/CRC)
Gelman, A. & Rubin, D.B. 1992, Statistical Science, 7, 457
Gettel, S., et al. 2012, ApJ, 745, 28
Girardi, L., Bressan, A., Bertelli, G., & Chiosi, C. 2000, A&AS, 141, 371
Gregory, P.C. 2005, ApJ, 631, 1198
Hatzes, A.P., Guenther, E.W., Endl, M., Cochran, W.D., Döllinger, M.P., & Bedalov, A. 2005, A&A, 437, 743
Hatzes, A.P., et al. 2006, A&A, 457, 335
Holman, M., Touma, J., & Tremaine, S. 1997, Nature, 386, 254
Izumiura, H. 1999, in Proc. 4th East Asian Meeting on Astronomy, ed. P.S. Chen (Kunming: Yunnan Observatory), 77
Johnson, J.A., et al. 2010, ApJ, 721, 153
Johnson, J.A., et al. 2011a, ApJS, 197, 26
Johnson, J.A., et al. 2011b, AJ, 141, 16
Jurić, M. & Tremaine, S. 2008, ApJ, 686, 603
Kambe, E., et al. 2002, PASJ, 54, 865
Kambe, E., et al. 2013, PASJ, 65, 15
Kurucz, R. L. 1993, Kurucz CD-ROM, No. 13 (Harvard-Smithsonian Center for Astrophysics)
Lee, B.-C., Han, I., Park, M.-G., Mkrtichian, D. E., & Kim, K.-M. 2012, A&A, 546, 5
Lejeune, T., & Schaerer, D. 2001, A&A, 366, 538
Liu, Y.-J., et al. 2008, ApJ, 672, 553

Lovis, C., & Mayor, M. 2007, A&A, 472, 657
Marois, C.. et al. 2008, Science, 322, 1348
Mayor, M. & Udry, S. 2008, Phys. Scr., 130, 014010
Marzari, F. & Weidenschilling, S. J, 2002, Icarus, 156, 570
Mazeh, T., Krymolowski, Y., & Rosenfeld, G. 1997, ApJ, 477, L103
Niedzielski, A., Gozdziewski, K., Wolszczan, A., Konacki, M., Nowak, G., & Zielinski, P. 2009a, ApJ, 693, 276
Niedzielski, A., Nowak, G., Adamow, M., & Wolszczan, A. 2009b, ApJ, 707, 768
Noyes, R.W., Hartmann, L.W., Baliunas, S. L., Duncan, D. K., & Vaughan, A. H. 1984, ApJ, 279, 763
Omiya, M., et al., 2009, PASJ, 61, 825
Omiya, M., et al., 2012, PASJ, 64, 34
Queloz, D. et al. 2001, A&A, 379, 279
Roberts, G.O., Gelman, A., & Gilks, W.R. 1997, Ann. Appl. Probability, 7, 110
Sato, B., Kambe, E., Takeda, Y., Izumiura, H., & Ando, H. 2002, PASJ, 54, 873
Sato, B., Kambe, E., Takeda, Y., Izumiura, H., Masuda, S., & Ando, H. 2005, PASJ, 57, 97
Sato, B., et al. 2007, ApJ, 661, 527
Sato, B., et al. 2010, PASJ, 62, 1063
Sato, B., et al. 2012, PASJ, 64, 135
Sato, B., et al. 2013, ApJ, 762, 9
Scargle, J. D. 1982, ApJ, 263, 835
Setiawan, J., et al. 2005, A&A, 437, 31
Siess, L., & Livio, M. 1999, MNRAS, 308, 1133
Takeda, Y., Ohkubo, M., & Sadakane, K. 2002, PASJ, 54, 451
Takeda, Y., Sato, B., & Murata, D., 2008, PASJ, 60, 781
Takeda, G., & Rasio, F.A. 2005, ApJ, 627, 1001
Wang, L., et al., 2012, RAA, 12, 84
Winn, J. N., Johnson, J.A., Albrecht, S., Howard, A.W., Marcy, G.W., Crossfield, I.J., & Holman, M.J., 2009, ApJL, 703, L99
Wittenmyer, R. A., Endl, M., Wang, L., Johnson, J. A., Tinney, C. G., & O'Toole, S. J. 2011, ApJ, 743, 184

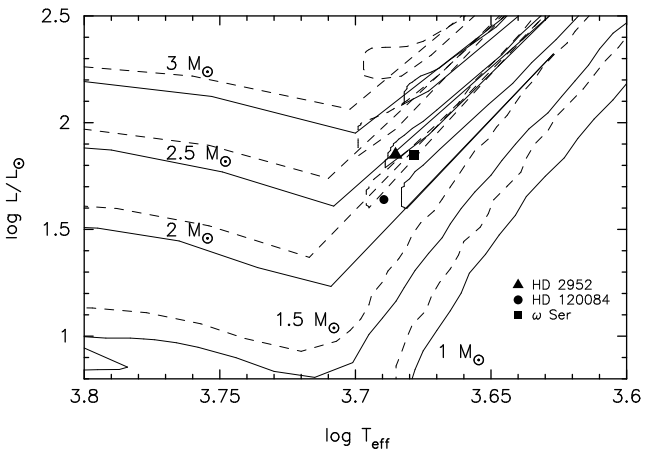

Fig. 1. HR diagram of the planet-harboring stars presented in this paper. Pairs of evolutionary tracks from Lejeune and Schaerer (2001) for stars with $Z = 0.02$ (solar metallicity; solid lines) and $Z = 0.008$ (dashed lines) of masses between 1 and 3 $M_{\odot}$ are also shown.

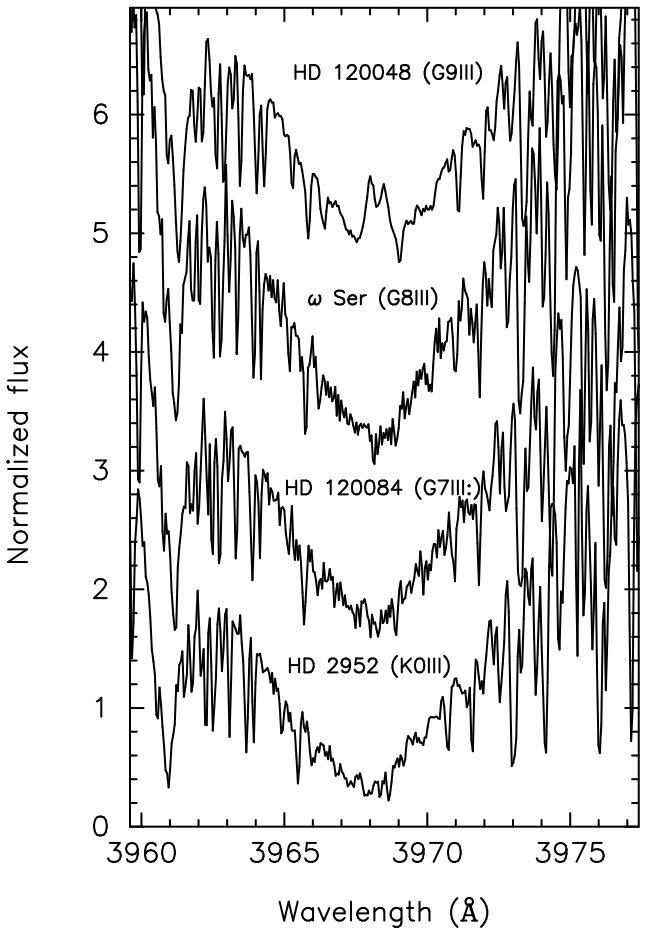

Fig. 2. Spectra in the region of Ca H lines. All of the stars show no significant core reversals in the lines compared to that in the chromospheric active star HD 120048. A vertical offset of about 0.8 is added to each spectrum.

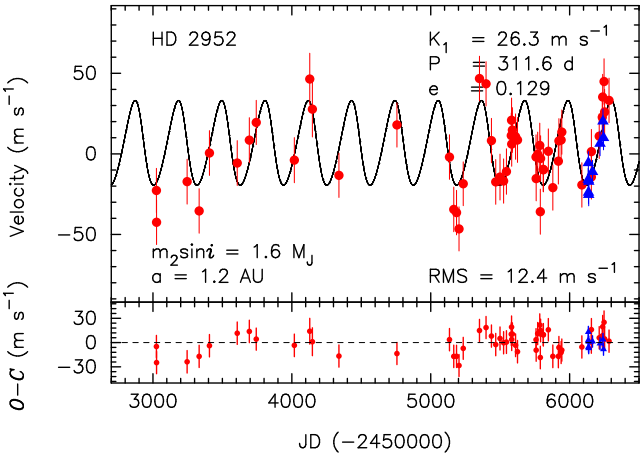

Fig. 3. *Top*: Radial velocities of HD 2952 observed at OAO. HIDES-Slit data are shown in filled red circles, and HIDES-Fiber data are filled blue triangles. The Keplerian orbit is shown by the solid line. The error bar for each point includes the stellar jitter. *Bottom*: Residuals to the orbital fit. The rms to the fit is 12.4 m s^{-1}.

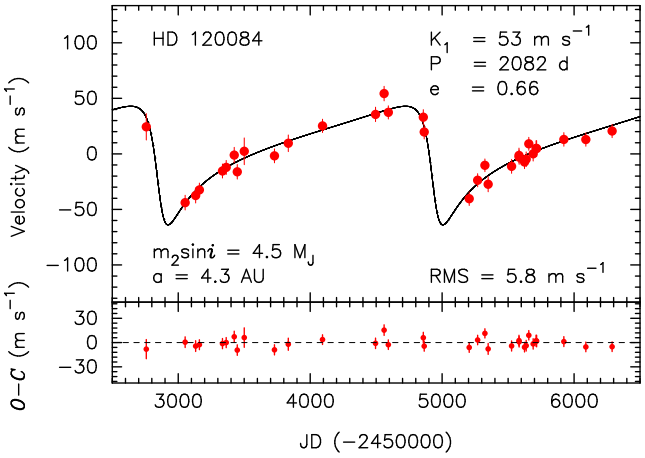

Fig. 5. *Top*: Radial velocities of HD 120084 observed at OAO. HIDES-Slit data are shown in filled red circles. The Keplerian orbit is shown by the solid line. The error bar for each point includes the stellar jitter. *Bottom*: Residuals to the orbital fit. The rms to the fit is 5.8 m s^{-1}.

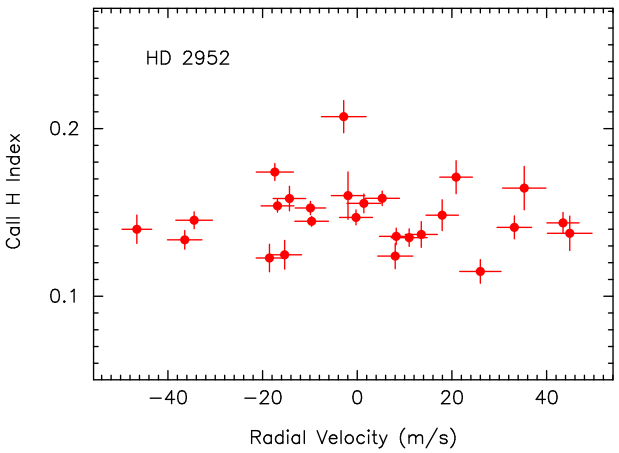

Fig. 4. CaII H index against radial velocity for HD 2952.

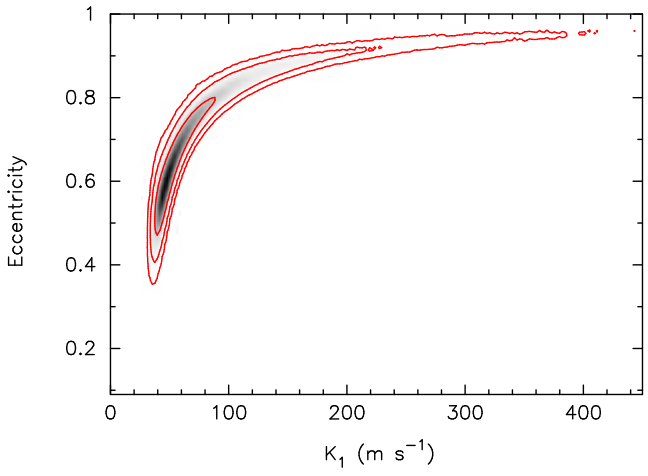

Fig. 6. Two dimensional PDF for eccentricity e and velocity semiamplitude K_1 for HD 120084. The red solid lines represent contours for 68.3%, 95.4%, and 99.73% confidence from inside to out.

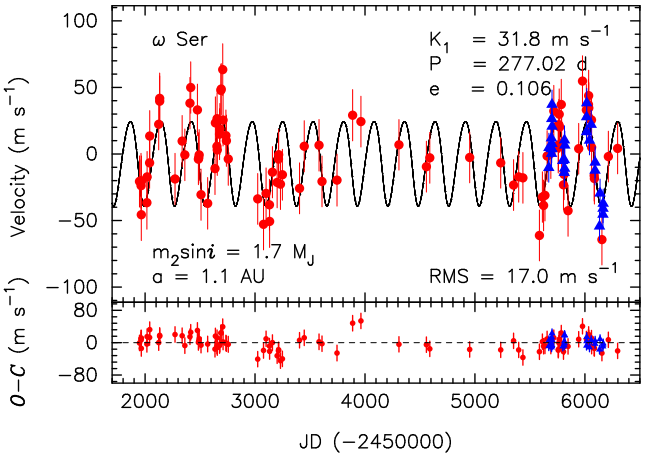

Fig. 7. *Top*: Radial velocities of ω Ser observed at OAO. HIDES-Slit data are shown in filled red circles, and HIDES-Fiber data are filled blue triangles. The Keplerian orbit is shown by the solid line. The error bar for each point includes the stellar jitter. *Bottom*: Residuals to the orbital fit. The rms to the fit is 17.0 m s^{-1}.

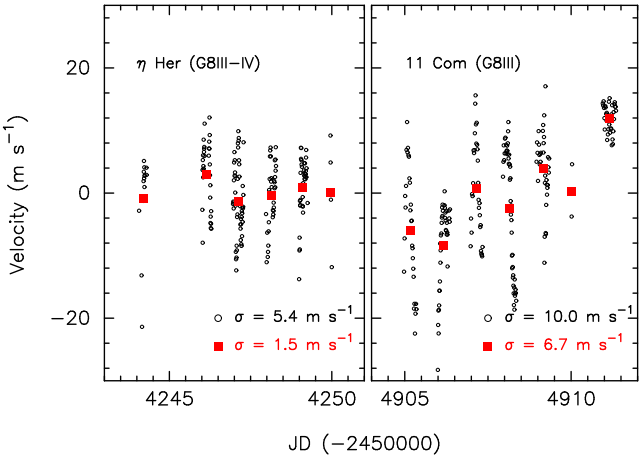

Fig. 10. Short-term radial velocity variations for G giants, η Her (left) and 11 Com (right). The radial velocity data are from Ando et al. (2010). Open circles are raw data and red squares are those binned over one night. An increasing velocity trend seen in 11 Com is caused by orbital motion (Liu et al. 2008), the RMS scatter of the binned data to which is 4.5 m s^{-1}.

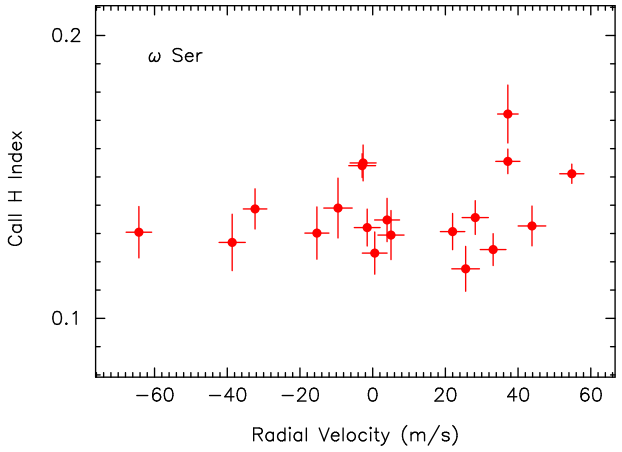

Fig. 8. CaII H index against radial velocity for ω Ser.

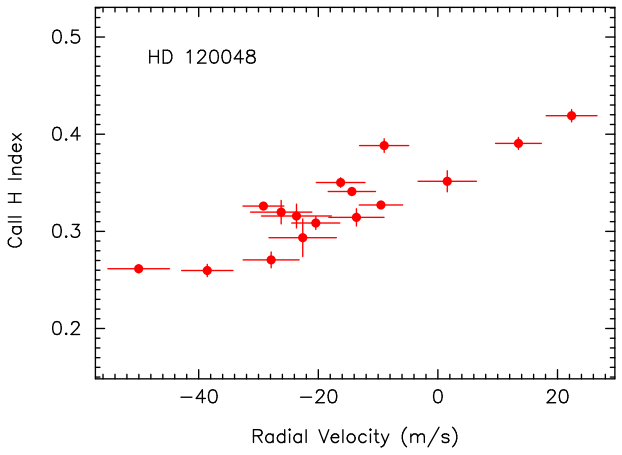

Fig. 9. CaII H index against radial velocity for HD 120048.

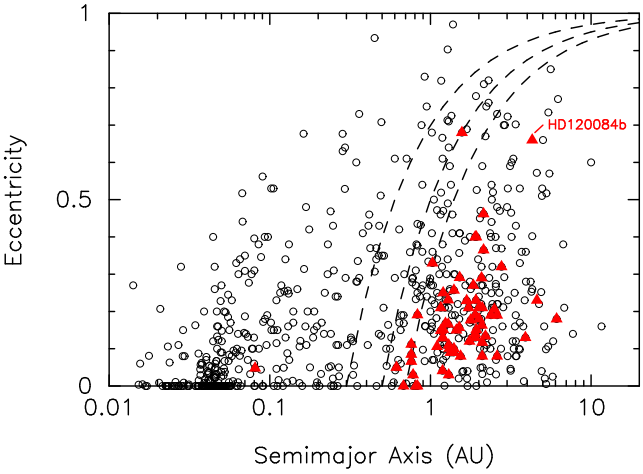

Fig. 11. Eccentricity distribution of exoplanets detected by radial velocity methods against semimajor axis. The data are from http://exoplanets.eu. Red triangles represent planets around evolved intermediate-mass ($\gtrsim 1.5 M_\odot$) stars. Dashed lines express the periastron distance ($q = a(1-e)$) of 0.3, 0.5, 0.7 AU, respectively, from the left. The planet with $e = 0.68$ and $a = 1.57$ AU is HD 102272c, which is in a double planet system (Niedzielski et al. 2009a).

Table 1. Stellar parameters

Parameter	HD 2952	HD 120084	ω Ser
Sp. Type	K0 III	G7 III:	G8 III
π (mas)	8.68±0.71	10.24±0.49	12.40±0.73
V	5.93	5.91	5.21
$B-V$	1.037	1.000	1.019
A_V	0.18	0.00	0.06
M_V	+0.44	+0.96	+0.49
$B.C.$	−0.32	−0.30	−0.35
$T_{\rm eff}$ (K)	4844±20	4892±22	4770±10
$\log g$ (cgs)	2.67±0.07	2.71±0.08	2.32±0.04
v_t (km s^{-1})	1.32±0.08	1.31±0.10	1.34±0.04
[Fe/H] (dex)	+0.00±0.04	+0.09±0.05	−0.24±0.02
L ($L_\odot$)	70.8	43.7	70.8
R ($R_\odot$)	12.02 (10.96–13.18)	9.12 (8.51–9.77)	12.30 (11.48–13.18)
M ($M_\odot$)	2.54 (2.45–2.66)	2.39 (2.09–2.45)	2.17 (1.88–2.38)
$v \sin i$ (km s^{-1})	1.92	2.44	1.89
$\sigma_{\rm HIP}$ (mag)	0.007	0.007	0.005

Note – The uncertainties of [Fe/H], $T_{\rm eff}$, $\log g$, and $v_{\rm t}$, are internal statistical errors (for a given dataset of Fe I and Fe II line equivalent widths) evaluated by the procedure described in subsection 5.2 of Takeda et al. (2002). Since these parameter values are sensitive to slight changes in the equivalent widths as well as to the adopted set of lines (Takeda et al. 2008) realistic ambiguities may be by a factor of $\sim$ 2–3 larger than these estimates from a conservative point of view (e.g., 50–100 K in $T_{\rm eff}$, 0.1–0.2 dex in $\log g$). Values in the parenthesis for stellar radius and mass correspond to the range of the values assuming the realistic uncertainties in $\Delta \log L$ corresponding to parallax errors in the Hipparcos catalog, $\Delta \log T_{\rm eff}$ of $\pm$0.01 dex ($\sim \pm$100 K), and Δ[Fe/H] of $\pm$0.1 dex. The resulting mass value may also appreciably depend on the chosen set of theoretical evolutionary tracks (e.g., the systematic difference as large as $\sim 0.5 M_\odot$ for the case of metal-poor tracks between Lejeune & Schaerer (2001) and Girardi et al. (2000)).

Table 2. Parameter Priors for MCMC Orbital Analysis

Parameter	Prior	Minimum	Maximum
P (days)	Jeffreys	1	10000
K_1 (m s^{-1})	Modified Jeffreys	0 ($K_a = 5$)	1000
e	Uniform	0	1
ω	Uniform	0	2π
χ	Uniform	0	1
V (m s^{-1})	Uniform	−100	100
s (m s^{-1})	Modified Jeffreys	0 ($s_a = 1$)	100

Table 3. Radial Velocities of HD 2952

JD (−2450000)	Radial Velocity (m s^{-1})	Uncertainty (m s^{-1})	Obs. Mode
3024.97290	−22.7	3.5	Slit
3025.97090	−42.4	3.7	Slit
3246.14274	−17.2	4.1	Slit
3332.97862	−35.4	3.7	Slit
3406.94360	0.5	4.0	Slit
3607.23421	−5.7	3.9	Slit
3694.19166	8.5	4.2	Slit
3744.01898	19.5	3.3	Slit
4018.30303	−3.9	4.3	Slit
4128.91328	46.5	8.8	Slit
4147.92413	27.8	11.0	Slit
4339.27515	−13.3	3.4	Slit
4757.00848	17.9	3.4	Slit
5135.22351	−2.0	3.7	Slit
5166.06192	−34.5	3.9	Slit
5185.98912	−36.4	3.6	Slit
5203.98979	−46.6	3.1	Slit
5233.95877	−18.5	2.8	Slit
5351.27989	46.7	3.8	Slit
5398.25033	43.5	3.4	Slit
5437.15263	8.2	3.5	Slit
5468.21069	−17.4	3.9	Slit
5499.00815	−14.4	5.1	Slit
5524.96261	−16.9	3.5	Slit
5545.07666	−11.0	4.7	Slit
5579.98277	11.4	4.5	Slit
5581.95150	20.9	3.5	Slit
5582.98312	6.1	3.4	Slit
5587.99681	14.8	4.0	Slit
5610.92984	10.7	4.6	Slit
5624.91445	8.6	4.0	Slit
5758.19046	−2.0	3.5	Slit
5759.20471	−15.3	3.6	Slit
5770.26968	−0.3	3.5	Slit
5785.28326	5.3	3.7	Slit
5789.19561	−35.9	4.3	Slit
5791.31690	−2.9	4.7	Slit
5810.31005	−9.6	3.6	Slit
5811.25892	−9.9	3.2	Slit
5847.04083	1.6	4.1	Slit
5879.06072	−20.9	4.4	Slit
5918.88801	−4.5	4.9	Slit
5922.97437	8.0	3.7	Slit
5938.92083	8.6	3.3	Slit
5943.88388	13.5	3.4	Slit
6088.28662	−19.3	3.7	Slit
6156.30600	−14.3	3.4	Slit
6157.21819	1.4	3.6	Slit
6213.20713	11.0	3.8	Slit
6235.00453	22.7	4.3	Slit
6238.13304	35.3	4.6	Slit
6247.98096	44.9	4.7	Slit
6252.07358	26.0	4.4	Slit
6283.88204	33.2	3.6	Slit

Table 3. (Continued.)

JD (−2450000)	Radial Velocity (m s^{-1})	Uncertainty (m s^{-1})	Obs. Mode
6134.27677	−9.1	2.5	Fiber
6135.19472	1.3	2.6	Fiber
6136.16962	−17.0	2.4	Fiber
6137.32056	−18.4	2.3	Fiber
6138.27673	−10.3	2.4	Fiber
6165.14597	−4.2	2.8	Fiber
6219.12083	13.4	4.0	Fiber
6239.98610	27.2	3.8	Fiber
6244.03652	16.9	3.7	Fiber

Table 4. Radial Velocities of HD 120084

JD (−2450000)	Radial Velocity (m s^{-1})	Uncertainty (m s^{-1})	Obs. Mode
2758.08834	24.4	10.8	Slit
3052.17823	−43.9	4.3	Slit
3131.98703	−37.5	4.4	Slit
3160.03439	−32.5	3.6	Slit
3335.31086	−15.4	3.9	Slit
3363.38688	−12.2	3.8	Slit
3424.14553	−1.1	4.8	Slit
3447.22989	−16.1	4.2	Slit
3500.09881	2.3	11.0	Slit
3729.35861	−1.8	3.8	Slit
3834.18777	9.5	5.6	Slit
4093.33261	25.2	3.3	Slit
4495.32067	35.5	4.1	Slit
4560.13449	54.3	4.2	Slit
4592.13620	37.4	3.2	Slit
4857.17673	33.1	4.5	Slit
4864.29286	19.7	3.8	Slit
5205.25700	−40.4	3.4	Slit
5269.20359	−23.8	3.1	Slit
5324.04791	−10.3	2.8	Slit
5349.06372	−27.3	4.6	Slit
5526.36838	−11.2	3.8	Slit
5582.23410	−1.4	4.3	Slit
5583.34207	−2.9	4.0	Slit
5624.30459	−7.3	3.2	Slit
5637.10714	−4.8	4.3	Slit
5657.10287	9.1	3.0	Slit
5690.13478	0.0	4.0	Slit
5712.07387	5.0	4.7	Slit
5716.03317	4.8	5.1	Slit
5922.30833	13.0	3.5	Slit
6089.02875	12.9	3.3	Slit
6288.33466	20.6	3.2	Slit

Table 5. Radial Velocities of ω Ser

JD (−2450000)	Radial Velocity (m s^{-1})	Uncertainty (m s^{-1})	Obs. Mode
1949.32661	−20.7	4.4	Slit
1963.23330	−20.0	8.4	Slit
1963.31681	−23.8	4.7	Slit
1965.33358	−45.6	5.1	Slit
1966.30201	−20.7	4.3	Slit
2016.29162	−36.6	7.0	Slit
2018.19403	−17.2	3.8	Slit
2041.13940	−6.7	3.9	Slit
2042.11952	13.5	3.8	Slit
2123.98945	22.3	4.4	Slit
2132.99172	39.6	3.0	Slit
2133.00942	41.8	3.2	Slit
2272.35035	−18.8	4.6	Slit
2337.31840	9.7	4.4	Slit
2361.31453	−0.6	5.1	Slit
2408.08042	38.2	4.9	Slit
2415.09944	49.9	4.9	Slit
2475.99488	33.1	4.9	Slit
2485.04153	−3.9	4.0	Slit
2488.04647	−2.9	3.3	Slit
2492.01853	−0.7	3.3	Slit
2508.98656	−30.6	4.5	Slit
2568.89966	−37.1	5.1	Slit
2635.37474	−11.0	5.6	Slit
2639.38303	23.3	5.8	Slit
2653.37319	5.7	4.3	Slit
2654.38879	26.5	4.8	Slit
2656.34630	3.1	4.2	Slit
2677.35725	14.9	4.0	Slit
2680.34513	18.8	4.2	Slit
2689.32234	47.8	5.1	Slit
2692.28082	48.8	4.1	Slit
2706.26453	63.4	5.3	Slit
2709.31474	25.5	5.3	Slit
2735.22182	13.8	4.6	Slit
2739.27107	9.9	4.5	Slit
2756.25351	−3.8	6.4	Slit
3024.37398	−33.7	3.8	Slit
3077.25145	−52.8	4.4	Slit
3100.25088	−29.6	4.1	Slit
3131.13458	−38.2	4.1	Slit
3132.27689	−50.6	5.9	Slit
3158.18452	−13.7	4.5	Slit
3201.07394	−21.3	3.8	Slit
3213.02084	−3.8	4.0	Slit
3215.04862	−0.6	3.8	Slit
3231.00895	−22.7	3.8	Slit
3248.98212	−15.6	3.8	Slit
3404.34420	−25.8	3.9	Slit
3447.25348	5.8	4.3	Slit
3581.98388	6.6	5.0	Slit
3609.01868	−20.6	3.8	Slit
3745.37391	−19.6	5.6	Slit
3887.22571	29.1	4.5	Slit
3962.95693	24.3	3.7	Slit

Table 5. (Continued.)

JD (−2450000)	Radial Velocity (m s^{-1})	Uncertainty (m s^{-1})	Obs. Mode
4308.99011	6.9	3.2	Slit
4558.19006	−9.5	3.9	Slit
4589.19334	−2.9	3.7	Slit
4952.20424	−2.6	3.6	Slit
5234.30043	−6.7	3.3	Slit
5351.02660	−23.3	3.8	Slit
5398.04047	−17.2	3.4	Slit
5435.96330	−17.9	3.6	Slit
5586.31423	−61.2	3.9	Slit
5613.33791	−32.3	3.2	Slit
5624.36003	−38.6	3.6	Slit
5636.34089	−31.1	4.3	Slit
5656.22321	−1.5	3.6	Slit
5690.16462	0.6	3.4	Slit
5717.09514	32.2	4.8	Slit
5757.06063	4.8	3.8	Slit
5759.08554	6.7	3.7	Slit
5763.01162	22.0	3.4	Slit
5766.00806	29.8	3.7	Slit
5770.05598	20.2	3.8	Slit
5785.01129	37.2	2.8	Slit
5787.96807	8.2	4.5	Slit
5804.95034	−23.2	2.8	Slit
5809.94684	−15.3	3.3	Slit
5846.89877	−42.6	4.3	Slit
5943.37404	4.0	3.4	Slit
5978.36886	54.8	3.3	Slit
6013.26399	33.1	3.5	Slit
6030.28218	28.2	3.6	Slit
6032.20041	37.2	3.3	Slit
6034.20383	43.8	3.8	Slit
6035.31167	34.6	3.6	Slit
6060.10402	25.6	3.8	Slit
6061.09811	5.0	3.6	Slit
6084.08376	−16.2	4.2	Slit
6086.18326	−18.4	4.1	Slit
6154.97320	−64.3	3.5	Slit
6212.90005	−2.0	3.7	Slit
6297.38811	4.2	3.7	Slit
5671.20537	−9.5	3.2	Fiber
5672.26886	5.5	3.3	Fiber
5695.15717	4.6	2.8	Fiber
5695.28079	12.8	2.9	Fiber
5696.06702	1.1	2.8	Fiber
5696.10871	4.9	2.6	Fiber
5697.08506	5.0	2.5	Fiber
5698.21953	27.3	4.0	Fiber
5700.15563	8.6	3.1	Fiber
5701.02381	38.0	3.1	Fiber
5701.12905	21.5	2.6	Fiber
5797.95807	−4.2	2.4	Fiber
5811.94795	−13.2	2.2	Fiber
5812.96282	−3.5	2.4	Fiber

Table 5. (Continued.)

JD (−2450000)	Radial Velocity (m s^{-1})	Uncertainty (m s^{-1})	Obs. Mode
5813.94961	11.3	2.8	Fiber
5814.93863	−10.0	3.0	Fiber
5816.97108	7.3	2.7	Fiber
6014.22031	17.4	3.1	Fiber
6015.17803	28.6	3.0	Fiber
6016.16312	39.2	3.5	Fiber
6041.26690	11.1	3.2	Fiber
6057.22610	23.0	2.7	Fiber
6092.06771	−11.5	3.5	Fiber
6093.16308	−5.5	5.3	Fiber
6133.01204	−53.5	2.5	Fiber
6137.96888	−28.7	2.2	Fiber
6164.00431	−44.6	2.5	Fiber
6164.99025	−40.1	2.6	Fiber
6165.99606	−36.3	2.8	Fiber

Table 6. Orbital Parameters

Parameter	HD 2952 b	HD 120084 b	ω Ser b
P (days)	$311.6^{+1.7}_{-1.9}$	2082^{+24}_{-35}	$277.02^{+0.52}_{-0.51}$
K_1 (m s^{-1})	$26.3^{+3.8}_{-3.4}$	53^{+33}_{-11}	$31.8^{+2.3}_{-2.3}$
e	$0.129^{+0.099}_{-0.085}$	$0.66^{+0.14}_{-0.10}$	$0.106^{+0.079}_{-0.069}$
ω (deg)	64^{+56}_{-48}	117^{+12}_{-9}	132^{+34}_{-52}
T_p (JD−2,450,000)	112^{+64}_{-54}	774^{+80}_{-61}	22^{+27}_{-38}
$s_{\rm slit}$ (m s^{-1})	$13.3^{+1.6}_{-1.4}$	$5.0^{+1.2}_{-1.0}$	$18.7^{+1.6}_{-1.4}$
$s_{\rm fiber}$ (m s^{-1})	$6.5^{+2.6}_{-1.8}$	–	$10.4^{+1.8}_{-1.4}$
$\Delta{\rm RV}_{\rm f-s}$ (m s^{-1})	$6.9^{+3.8}_{-3.8}$	–	$0.84^{+2.9}_{-2.9}$
$a_1 \sin i$ (10^{-3}AU)	$0.74^{+0.10}_{-0.09}$	$7.7^{+2.4}_{-1.1}$	$0.804^{+0.057}_{-0.057}$
$f_1(m)$ ($10^{-7} M_\odot$)	$0.0057^{+0.0027}_{-0.0019}$	$0.14^{+0.18}_{-0.05}$	$0.0090^{+0.0021}_{-0.0018}$
$m_2 \sin i$ ($M_{\rm J}$)	1.6	4.5	1.7
a (AU)	1.2	4.3	1.1
$N_{\rm slit}$	54	33	94
$N_{\rm fiber}$	9	–	29
RMS (m s^{-1})	12.4	5.8	17.0

Table 7. Bisector Quantities

Bisector Quantities	HD 2952	HD 120084	ω Ser	HD 120048
Bisector Velocity Span (BVS) (m s^{-1})	−6.0±2.9	1.3±3.7	2.1±4.2	2.0±5.1
Bisector Velocity Curvature (BVC) (m s^{-1})	1.2±1.3	−0.9±2.2	0.6±2.1	−4.8±3.0
Bisector Velocity Displacement (BVD) (m s^{-1})	−69.6±5.1	−70.0±6.2	−102.4±8.5	−68.0±8.8